

Direct calculation of the ZZ-interaction rates in the multi-mode circuit-QED

Firat Solgun and Srikanth Srinivasan

IBM Quantum, IBM T. J. Watson Research Center, Yorktown Heights, NY 10598 USA

Hamiltonians of the superconducting qubits of Transmon type involve non-zero ZZ-interaction terms due to their finite and small anharmonicities. These terms might lead to the unwanted accumulation of spurious phases during the execution of the two-qubit gates. Exact calculation of the ZZ-interaction rates requires the full diagonalization of the circuit Hamiltonians which very quickly becomes computationally demanding as the number of the modes in the coupler circuit increases. Here we propose a direct analytical method for the accurate estimation of the ZZ-interaction rates between low-anharmonicity qubits in the dispersive limit of the multi-mode circuit-QED. We observe very good agreement between the predictions of our method and the measurement data collected from the multi-qubit devices. Our method being an extension of our previous work in [1] is a new addition to the toolbox of the quantum microwave engineers as it relates the ZZ-interaction rates directly to the entries of the impedance matrix defined between the qubit ports.

I. INTRODUCTION

Superconducting quantum processors are one of the leading platforms in the race to achieve fault-tolerant quantum computation. Several important performance figures such as the qubit coherence times, gate and measurement fidelities have been steadily improving in the last two decades and they reached [2–6] the error threshold levels as required by the quantum error-correction protocols [7, 8]. However keeping the same performance for the individual components while scaling the circuits up remains a big engineering challenge [9].

Superconducting qubits are made of Josephson junctions which are lossless two-terminal circuit elements. Josephson junctions provide the non-linearity needed to obtain the qubit modes by allowing the “supercurrent” to flow between their terminals by tunneling while introducing minimal loss [10]. The most popular superconducting qubit Transmon [11] is obtained by shunting the Josephson junction with a relatively large capacitor. As such the Transmon qubit is a nonlinear oscillator with small anharmonicity to make it insensitive to charge fluctuations that cause dephasing. Transmon qubits are often modeled as multi-level quantum Duffing oscillators and they are designed to interact with each other and with their environment in the circuit-QED architecture [12, 13].

In the circuit-QED architecture qubit interactions are mediated by the linear and passive microwave environment that the Josephson junctions are embedded in. Qubits are typically coupled to each other and to the control/measurement electronics by the help of microwave components constructed out of CPW transmission lines and their bare interactions with the internal modes of these structures are of the exchange energy type. When the strength of these interactions is smaller than the detuning of the qubits from the internal modes the system is said to be operated in the dispersive regime. It was shown in [1] that in the dispersive limit multi-mode circuit-QED systems can be described by an effective Hamiltonian of Duffing oscillators whose interactions with each other and with the drive lines are directly related to the entries

of the impedance matrix defined between the qubit and drive ports.

However when one reduces the effective Hamiltonian of the circuit to a qubit Hamiltonian by eliminating the higher levels of the Duffing oscillators non-zero ZZ-interaction (Ising type) terms are generated due to the finite and small anharmonicities of the qubits in addition to the main exchange interaction terms [14]. These ZZ-interaction terms might be a nuisance for some two-qubit gate schemes such as the CR-gate [15] which is the most popular microwave activated gate that creates the entanglement between the qubits via the ZX-interaction. A non-zero ZZ-term in the qubit Hamiltonian will cause spurious phase accumulations in the presence of spectator qubits and will lead to the loss of the gate fidelity.

The suppression of the ZZ-term in the qubit Hamiltonians has recently been studied actively to improve two-qubit gate fidelities. In [16] a coupler design is proposed that consists of two arms one of which is frequency tunable and the coupler suppresses the ZZ-term by the interference of the interaction paths through each arm. It is shown that the system can be tuned to a point where the ZZ-interaction becomes zero but the effective exchange interaction J remains finite. Originally a similar topology was used in [17] to make exchange interaction zero. Other approaches include the use of qubits of opposite anharmonicities [18] and of tunable qubits [19] to cancel the ZZ-interaction. More recently with a circuit topology similar to [16] but using non-tunable elements only [20] showed that it is possible to suppress the ZZ-term over a relatively large band while keeping a finite J -coupling rate that is useful for running the CR-gate [15]. Although a source of cross-talk for the CR-gate ZZ-interactions can also mediate controlled-phase (CZ) gates [21–24].

In this paper we develop a method for the accurate estimation of the ZZ rates between Transmon type low anharmonicity qubits in the multi-mode circuit-QED. The frequency dependence of the ZZ rates is captured by the impedance entries connecting the qubit ports hence the high computational cost of diagonalizing multi-mode Hamiltonians is avoided making the microwave engineering [25] of multi-mode quantum couplers streamlined.

In Section (II) we start with the summary of the theory [1] that our method is based on. The method is described in Section (III). The predictions of our theory are validated with numerical simulations on the example circuits in Section (IV). In Section (V) we compare the experimental data collected from multi-qubit devices to the ZZ values calculated with our method.

II. THE EFFECTIVE HAMILTONIAN

We start with an overview of the results in [1] as our calculations for the estimation of the ZZ rates in the next section will be performed in the reference frame given by the effective Hamiltonian derived in [1]. We assume that the quantum device under study consists of Transmon qubits connected to each other and to the read-out/control lines with the help of linear and passive microwave components such as transmission lines. For such systems the following effective Hamiltonian is derived in [1] in the dispersive limit of the circuit-QED:

$$\hat{\mathcal{H}}/\hbar = \hat{H}_Q + \hat{H}_X + \hat{H}_R \quad (1)$$

$\hat{\mathcal{H}}$ is obtained by block-diagonalizing the initial system Hamiltonian in Eq. (17) of [1] by applying a Schrieffer-Wolff transformation. \hat{H}_Q collects the terms corresponding to the qubit subspace:

$$\hat{H}_Q = \hat{H}_Q^D + \hat{H}_Q^J + \hat{H}_Q^V$$

where \hat{H}_Q^D is the diagonal part:

$$\hat{H}_Q^D = \sum_{i=1}^N \omega_i \hat{b}_i^\dagger \hat{b}_i + \frac{\delta_i}{2} \hat{b}_i^\dagger \hat{b}_i (\hat{b}_i^\dagger \hat{b}_i - 1) \quad (2)$$

which is the quantum Hamiltonian of N Duffing oscillators of frequencies ω_i 's, anharmonicities δ_i 's and annihilation(creation) operators \hat{b}_i (\hat{b}_i^\dagger)'s; for $1 \leq i \leq N$. The anharmonicity δ_i of the qubit i is given by [1]

$$\delta_i = -E_C^{(i)} \left(\frac{\omega_{J_i}}{\omega_i} \right)^2 = -\frac{E_C^{(i)}}{1 - 2E_C^{(i)}/\omega_i} \quad (3)$$

where $E_C^{(i)}$ is the charging energy of the i -th qubit given by $E_C^{(i)} = \frac{e^2}{2C_i}$, C_i is the total Transmon shunting capacitance of the qubit i ; for $1 \leq i \leq N$ and $\omega_{J_i} = 1/\sqrt{L_{J_i}C_i}$; L_{J_i} being the bare junction inductance corresponding to the qubit i .

Exchange couplings between qubits is given by the term \hat{H}_Q^J

$$\hat{H}_Q^J = \sum_{i,j} J_{ij} (\hat{b}_i \hat{b}_j^\dagger + \hat{b}_i^\dagger \hat{b}_j) \quad (4)$$

where the following formula is derived in [1] for the exchange coupling J_{ij} between qubit modes i and j

$$J_{ij} = -\frac{1}{4} \sqrt{\frac{\omega_i \omega_j}{L_i L_j}} \text{Im} \left[\frac{Z_{ij}(\omega_i)}{\omega_i} + \frac{Z_{ij}(\omega_j)}{\omega_j} \right] \quad (5)$$

where Z_{ij} is the impedance entry connecting the qubit port i to the qubit port j . Qubit ports are defined across the Josephson junctions of the Transmon qubits: port currents are the currents flowing through and the port voltages are the voltages developed across the Josephson junctions. L_i is the inductance of the i -th qubit and is related to the bare junction inductance L_{J_i} by $L_i = L_{J_i}/(1 - \frac{2E_C^{(i)}}{\hbar\omega_i})$.

The term \hat{H}_Q^V couples the qubits to the voltage drives and is given by

$$\hat{H}_Q^V = \sum_{i=1}^N \sum_{d=1}^{N_D} \varepsilon_{id} (\hat{b}_i - \hat{b}_i^\dagger) V_d \quad (6)$$

Here V_d is the voltage source driving the d -th drive line and there are N_D voltage sources in total. ε_{id} determines the coupling rate of the i -th qubit to the voltage source V_d

$$\varepsilon_{id} = \sqrt{\frac{\omega_i}{2\hbar L_i}} \text{Im} [Z_{i,p(d)}(\omega_i)] \frac{e^{i\theta_d} C_{p(d)}}{\sqrt{1 + \omega_d^2 Z_0^2 C_{p(d)}^2}} \quad (7)$$

where $Z_{i,p(d)}(\omega_i)$ is the impedance entry (evaluated at the frequency ω_i of the qubit i) connecting the qubit port i to the drive port $p(d)$ corresponding to the voltage source V_d . $C_{p(d)}$ is the capacitance shunting the drive port $p(d)$ and Z_0 is the characteristic impedance of the drive line. ω_d is the frequency of the voltage source V_d which is assumed to be a pure sinusoidal signal for simplicity. $\theta_d = \frac{\pi}{2} - \arctan(\omega_d Z_0 C_{p(d)})$ is the phase factor corresponding to V_d . See [1] for the details about the circuit model (the multiport Cauer network) used to define the qubit and drive ports.

\hat{H}_R collects the terms corresponding to the modes of the linear passive environment that the qubits are embedded in

$$\hat{H}_R = \hat{H}_R^D + \hat{H}_R^J + \hat{H}_R^V \quad (8)$$

where \hat{H}_R^D is the diagonal part given by

$$\hat{H}_R^D = \sum_{k=1}^M \omega_{R_k} \hat{a}_k^\dagger \hat{a}_k + \frac{\chi_{kk}^{(R)}}{2} \hat{a}_k^\dagger \hat{a}_k (\hat{a}_k^\dagger \hat{a}_k - 1) \quad (9)$$

Here it is assumed that there are M internal modes with the annihilation(creation) operators $\hat{a}_k^{(\dagger)}$'s and frequencies ω_{R_k} 's. We note that the internal modes have acquired anharmonicities $\chi_{kk}^{(R)}$'s generated by the junction

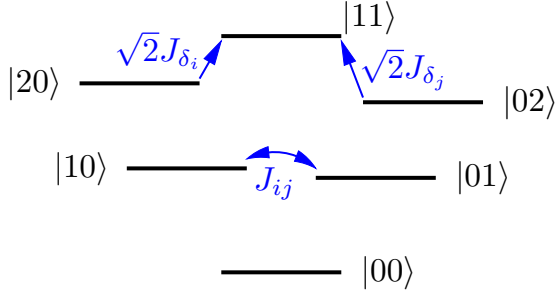


Figure 1. State diagram of the two Transmon qubits coupled with exchange coupling as given in Eq. (5). The couplings J_{δ_i} , J_{δ_j} of the second excited states $|20\rangle$, $|02\rangle$ of the qubits to the state $|11\rangle$ are updated with the treatment of the higher-order terms. Only states with up to two qubit excitations are shown and $|\Delta_{ij}| < |\delta_i|, |\delta_j|$ i.e. the straddling regime assumed for the detuning $\Delta_{ij} = \omega_i - \omega_j$ between the qubits i and j .

non-linearities and described by the self-Kerr terms in the Eq. (9) above.

Similar to the case for the qubit modes the term \hat{H}_R^J in Eq. (8) gives the exchange coupling $J_{kk'}$ between the internal modes k and k'

$$\hat{H}_R^J = \sum_{k,k'} J_{kk'} (\hat{a}_k \hat{a}_{k'}^\dagger + \hat{a}_k^\dagger \hat{a}_{k'}) \quad (10)$$

and the term \hat{H}_R^V couples the internal modes to the voltage drives

$$\hat{H}_R^V = \sum_{k=1}^M \sum_{d=1}^{N_D} \varepsilon_{kd} (\hat{a}_k - \hat{a}_k^\dagger) V_d \quad (11)$$

\hat{H}_χ holds the Kerr-type coupling terms left after the block-diagonalization. In particular the terms generating the qubit state dependent frequency shifts χ_{ik} 's in the readout resonator frequencies are contained in \hat{H}_χ given by

$$\hat{H}_\chi = \sum_{i=1}^N \sum_{k=1}^M \chi_{ik} \hat{b}_i^\dagger \hat{b}_i \hat{a}_k^\dagger \hat{a}_k \quad (12)$$

III. CALCULATION OF THE ZZ-INTERACTION RATE

The exchange coupling J_{ij} in Eq. (5) between qubits i and j can be diagonalized to get the following qubit Hamiltonian [14] (with $\hbar = 1$)

$$\hat{H}_Q = -\frac{(\omega_{10} + \omega_{ZZ}/2)}{2} \hat{Z} \hat{I} - \frac{(\omega_{01} + \omega_{ZZ}/2)}{2} \hat{I} \hat{Z} + \frac{\omega_{ZZ}}{4} \hat{Z} \hat{Z} \quad (13)$$

where $\omega_{10} = \omega_i + J_{ij}^2 / \Delta_{ij}$ and $\omega_{01} = \omega_j - J_{ij}^2 / \Delta_{ij}$ are the dressed qubit frequencies, $\Delta_{ij} = \omega_i - \omega_j$ the detuning between the qubits i and j and the ZZ-interaction rate ω_{ZZ} is shown to be [14]

$$\omega_{ZZ} = \omega_{11} - \omega_{10} - \omega_{01} \quad (14)$$

$$= -\frac{2J_{ij}^2(\delta_i + \delta_j)}{(\Delta_{ij} + \delta_i)(\delta_j - \Delta_{ij})} \quad (15)$$

However the accuracy of this formula can be improved significantly if one inspects more closely the higher order terms that are often dropped with a Rotating-Wave Approximation and include in the treatment the terms that are rotating at much slower frequencies. Such terms will bring corrections to the couplings between the second excited states of the qubits $|20\rangle$, $|02\rangle$ and the $|11\rangle$ state as shown in the state diagram in Fig. (1). Note that we have $J_{\delta_i} = J_{\delta_j} = J_{ij}$ in the formula in Eq. (15) since the higher order corrections are not taken into account in its derivation. To find the higher order corrections we borrow here the fourth order expansion of the cosine potentials of the Josephson junctions used in Eq. (115) of [1] after normal-ordering as

$$\begin{aligned} \hat{H}_\beta = & -\sum_{pp'qq'} \beta_{pp'qq'} (6\hat{a}_p^\dagger \hat{a}_{p'}^\dagger \hat{a}_q \hat{a}_{q'} + 4\hat{a}_p^\dagger \hat{a}_{p'}^\dagger \hat{a}_q^\dagger \hat{a}_{q'} + 4\hat{a}_p^\dagger \hat{a}_{p'} \hat{a}_q \hat{a}_{q'} \\ & + \hat{a}_p \hat{a}_{p'} \hat{a}_q \hat{a}_{q'} + \hat{a}_p^\dagger \hat{a}_{p'}^\dagger \hat{a}_q^\dagger \hat{a}_{q'}^\dagger) \end{aligned} \quad (16)$$

This expansion was originally given in [26] in a frame different than our block-diagonal frame. Anharmonicity terms in the diagonal Duffing Hamiltonian in Eq. (2) and the χ -shift term \hat{H}_χ in the Hamiltonian in Eq. (1) are both generated by \hat{H}_β in Eq. (16). To obtain the corrections to the couplings between $|20\rangle$, $|02\rangle$ and $|11\rangle$ states as shown in Fig. (1) we need to consider the terms $\hat{b}_i^\dagger \hat{b}_j^\dagger \hat{b}_i \hat{b}_j$, $\hat{b}_j^\dagger \hat{b}_i^\dagger \hat{b}_j \hat{b}_i$ and their Hermitian conjugates $\hat{b}_i^\dagger \hat{b}_i^\dagger \hat{b}_i \hat{b}_j$, $\hat{b}_j^\dagger \hat{b}_j^\dagger \hat{b}_j \hat{b}_i$; respectively in Eq. (16) above (\hat{b} denotes qubit operators in Eq. (16)). Note that these terms are rotating (if one goes to the interaction picture for example) at the frequency of qubit detuning Δ_{ij} which is much slower compared to the other terms. The weights of these terms are $\delta_i \sqrt{\frac{\omega_i}{\omega_j}} \alpha_{ij}$ and $\delta_j \sqrt{\frac{\omega_j}{\omega_i}} \alpha_{ji}$ respectively with

$$\alpha_{ij} = \frac{Z_{ji}^{-1}}{2(\omega_j^2 - \omega_i^2)} \text{Im} [(\omega_i^2 - 2\omega_j^2) Z_{ij}(\omega_j) + \omega_i \omega_j Z_{ij}(\omega_i)] \quad (17)$$

where we defined the “cross characteristic impedance” $Z_{ij} = \sqrt{L_i/C_j}$. The expression above is an update to the expression for α_{ij} originally given in Eq. (121) of [1] and is calculated using the total coordinate transformation $\alpha = \mathbf{T} \exp(\mathbf{S})$ of [1]. See Appendix (VII A) for the details of the derivation of the expression for α_{ij} in Eq. (17).

Using Eq. (17) together with Eq. (5) above we can now write

$$J_{\delta_i} = -\frac{1}{4} \sqrt{\frac{\omega_i \omega_j}{L_i L_j}} \text{Im} \left[\alpha_{\delta_i}^{(i)} \frac{Z_{ij}(\omega_i)}{\omega_i} + \alpha_{\delta_i}^{(j)} \frac{Z_{ij}(\omega_j)}{\omega_j} \right] \quad (18)$$

$$J_{\delta_j} = -\frac{1}{4} \sqrt{\frac{\omega_i \omega_j}{L_i L_j}} \text{Im} \left[\alpha_{\delta_j}^{(i)} \frac{Z_{ij}(\omega_i)}{\omega_i} + \alpha_{\delta_j}^{(j)} \frac{Z_{ij}(\omega_j)}{\omega_j} \right] \quad (19)$$

where the correction factors $\alpha_{\delta_i}^{(i)}$, $\alpha_{\delta_i}^{(j)}$, $\alpha_{\delta_j}^{(i)}$, $\alpha_{\delta_j}^{(j)}$ are given by

$$\alpha_{\delta_i}^{(i)} = 1 + 2 \frac{\omega_i \delta_i}{(\omega_i^2 - \omega_j^2)} \quad (20)$$

$$\alpha_{\delta_i}^{(j)} = 1 - 2 \frac{\omega_i \delta_i}{(\omega_i^2 - \omega_j^2)} + 4 \frac{\delta_i}{\omega_i} \quad (21)$$

$$\alpha_{\delta_j}^{(i)} = 1 + 2 \frac{\omega_j \delta_j}{(\omega_i^2 - \omega_j^2)} + 4 \frac{\delta_j}{\omega_j} \quad (22)$$

$$\alpha_{\delta_j}^{(j)} = 1 - 2 \frac{\omega_j \delta_j}{(\omega_i^2 - \omega_j^2)} \quad (23)$$

Hence we can update the perturbative formula in (15) for the ZZ-rate as

$$\omega_{ZZ} = 2 \frac{J_{\delta_i}^2(\delta_j - \Delta_{ij}) + J_{\delta_j}^2(\delta_i + \Delta_{ij})}{(\Delta_{ij} + \delta_i)(\Delta_{ij} - \delta_j)} \quad (24)$$

See Appendix (VII B) for the derivation of the expressions given in Eqs. (18) and (19) for J_{δ_i} and J_{δ_j} .

There is one more term in the expansion in Eq. (16) that we need to consider that contributes to the value of the ZZ-rate. This term is of the form $\hat{b}_i^\dagger \hat{b}_j^\dagger \hat{b}_i \hat{b}_j$ which is also called as the 'cross-Kerr' term. Its contribution to the ZZ-rate is usually small in the dispersive region. Its value can be calculated by working out the weight coefficients $\beta_{pp'qq'}$ in (16) and is given by

$$\omega_{ZZ}^{(K)} = 2\delta_i \left(\frac{\omega_i}{\omega_j} \right) \alpha_{ij}^2 + 2\delta_j \left(\frac{\omega_j}{\omega_i} \right) \alpha_{ji}^2 \quad (25)$$

Finally we introduce another parameter that was originally defined in Eq. (120) of [1]

$$\alpha_{ii} = \frac{1}{2} - \frac{3}{4} \text{Im}[Z_{ii}(\omega_i)]/Z_i - \frac{1}{4} \omega_i \text{Im}[Z'_{ii}(\omega_i)]/Z_i \quad (26)$$

where Z_i is the characteristic impedance of the i -th qubit and $Z'_{ii}(\omega_i) = \frac{dZ_{ii}(\omega)}{d\omega} \Big|_{\omega=\omega_i}$. Note that this is an updated version of the expression given in Eq. (120) of [1]. The coefficient α_{ii} gives the weight of the flux of qubit mode i on its own junction's phase. $\alpha_{ii} \cong 1$ in the dispersive region but it starts to deviate from one as the system exits the dispersive regime. Hence it is a good measure of how dispersive the system is. To include the corrections

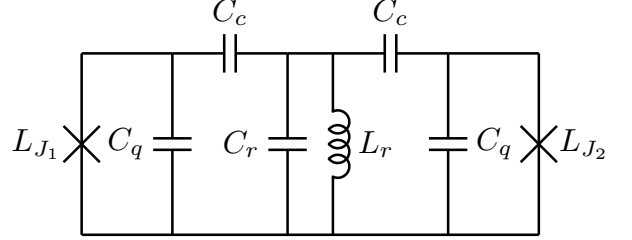


Figure 2. Single Mode Bus Circuit Diagram.

due to α_{ii} 's into our treatment all we need to do is to replace the charging energy $E_C^{(i)}$ in the expression for the anharmonicity in Eq. (3) with $\alpha_{ii}^2 E_C^{(i)}$; i.e. we need to update the anharmonicity δ_i of the qubit i given in Eq. (3) as follows

$$\delta_i = -\frac{\alpha_{ii}^2 E_C^{(i)}}{1 - 2\alpha_{ii}^2 E_C^{(i)}/\omega_i} \quad (27)$$

The updated formula above for the anharmonicity δ_i allows us to capture the frequency dependent changes due to the existence of the high frequency modes coupled to the qubits. Refer to the Appendix (VII A) for the derivation of the expressions given in Eqs. (26)-(27) for α_{ii} and δ_i .

IV. NUMERICAL EXAMPLES

We apply the method developed in the previous section for the direct calculation of the ZZ-rates to some simple circuits and compare the results to the exact diagonalization of the circuit Hamiltonians.

A. Single Mode Coupler

We start with the simple circuit shown in Fig. (2) consisting of two Transmon qubits coupled via a single mode shunt LC resonator bus. With $C_q = 60 \text{ fF}$, $C_c = 5 \text{ fF}$ we fix the qubits at 5.0 GHz and 5.2 GHz by adjusting the values of L_{J1} and L_{J2} accordingly and plot the ZZ-interaction rate as a function of the bus resonator frequency f_b in Fig. (3) using three different methods. The "naive" method of calculating the ZZ-rate is to plug-in the value of J_{12} calculated using Eq. (5) into (15). However we observe in Fig. (3) that there is significant discrepancy between this method (green curve labeled "Naive" in the legend) and the exact value of the ZZ-rate obtained with the numerical diagonalization of the circuit Hamiltonian (blue curve). And this discrepancy stays at a significant level even if we go deep into the dispersive region; i.e. as the bus frequency increases. However the accuracy is improved considerably when we apply the updated formula for the ZZ-rate in (24) by using the values

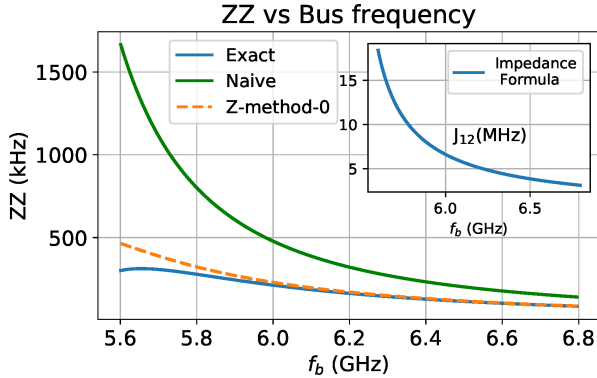


Figure 3. With qubits in Fig. (2) fixed at 5.0 GHz and 5.2 GHz ZZ-rates calculated using the formula in Eq. (15) (labeled as “Naive” in the figure legend) and the formula in Eq. (24) (labeled as “Z-method-0” in the figure legend) are compared to the exact value by the numerical diagonalization of the circuit Hamiltonian (labeled as “Exact” in the figure legend). Inset shows the level of J -coupling as a function of the bus frequency plotted applying the impedance formula in Eq. (5).

of J_{δ_1} and J_{δ_2} defined in Eqs. (18), (19). This is plotted as “Z-method-0” in Fig. (3) in orange color. The inset plot informs us about the exchange coupling strength J_{12} between the qubits as a function of the bus frequency calculated using the impedance formula in Eq. (5) for the same set of circuit parameters.

The accuracy of our calculation of the ZZ-rate can be improved further by adding the “cross-Kerr” contribution in Eq. (25) and the corrections due to the α_{ii} coefficients in Eqs. (26)-(27) into our treatment. The results are shown in Fig. (4) where we observe that the ZZ-rate calculated with the addition of the cross-Kerr term (brown curve) underestimates slightly the exact value (blue curve) whereas with the addition of α_{ii} corrections we obtain a very good agreement (dashed red) with true ZZ-values (blue) all the way down to $f_b = 5.6$ GHz which is only 400 MHz away from one of the qubits.

B. Two-Mode Coupler with Two J_{12} Zeros

Here we apply our method to a coupler consisting of two finite frequency modes. We start by artificially creating the following trans-impedance response

$$Z_{12}(\omega) = \frac{A(\omega_{z_1}^2 - \omega^2)(\omega_{z_2}^2 - \omega^2)}{\omega(\omega_{p_1}^2 - \omega^2)(\omega_{p_2}^2 - \omega^2)} \quad (28)$$

with three poles at DC, $\omega_{p_1} = 4.0$ GHz, $\omega_{p_2} = 6.25$ GHz and two zeros at $\omega_{z_1} = 4.5$ GHz and $\omega_{z_2} = 5.5$ GHz. The coefficient A is set to the value of -7.97×10^{10} . Assuming Transmon shunt capacitances of 65 fF we obtain the results in Fig. (5).

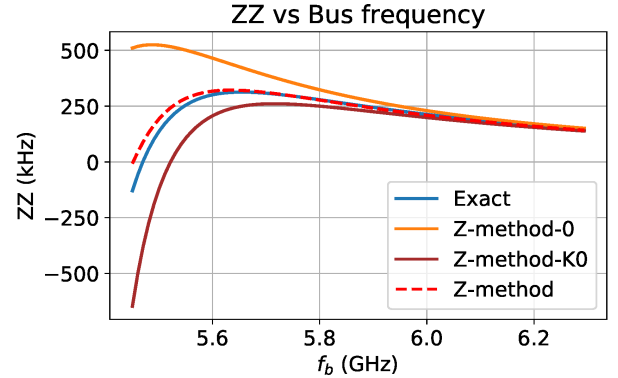


Figure 4. For the example circuit in Fig. (2) with qubits fixed at 5.0 and 5.2 GHz when only the cross-Kerr contribution in Eq. (25) is added (brown curved labeled “Z-method-K0” in the legend) to the updated ZZ-formula in (24) (orange) we underestimate the exact ZZ-values (blue) slightly. However when we also include the corrections due to the α_{ii} coefficients in Eqs. (26)-(27) we obtain the dashed red curve (labeled as “Z-method” in the figure legend) which agrees very well (even deep in the non-dispersive region) with the exact ZZ-values (blue) obtained by a full diagonalization of the circuit Hamiltonian.

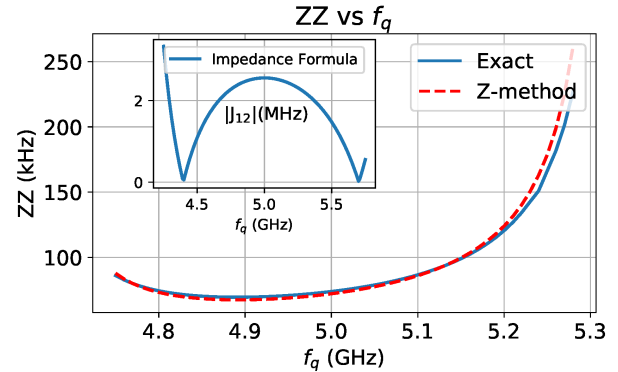


Figure 5. ZZ-rate for the trans-impedance Z_{12} defined in Eq. (28) with one of the qubits set to 5.0 GHz while the other qubit’s frequency is swept from 4.75 GHz to 5.30 GHz. The exchange coupling strength J_{12} is plotted in the inset for reference. Curves start diverging from each other after ~ 5.2 GHz because the qubit detuning becomes comparable to the anharmonicity.

C. Multi-Mode ZZ Cancellation Coupler

In this section we study an example of a multi-mode coupler designed to cancel the ZZ-interaction rate while keeping a finite J -coupling strength [20]. The coupler topology consists of two branches: one direct coupling branch of the form of a short segment of $\lambda/2$ CPW transmission line resonator and another branch of a short segment of CPW shunted to ground in the middle through a

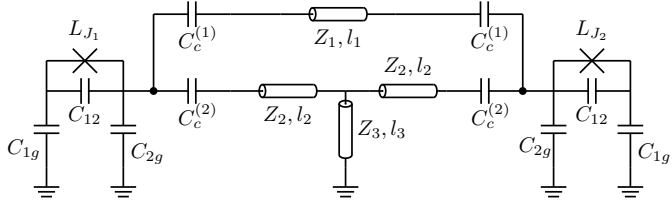


Figure 6. Multi-mode ZZ-Cancellation Coupler Circuit. The coupler consists of two arms: the top arm in the figure above is a short $\lambda/2$ CPW resonator whereas the bottom arm consists of a short CPW $\lambda/2$ section interrupted in the middle by a $\lambda/4$ resonator shorted to ground. Both arms run in parallel and are capacitively coupled to the same Transmon qubit pads. Circuit parameters are $C_{12} = 36$ fF, $C_{1g} = C_{2g} = 46$ fF, $C_c^{(1)} = 8$ fF, $C_c^{(2)} = 12$ fF. CPW transmission lines have lengths $l_1 = 1.0$ mm, $l_2 = 0.5$ mm, $l_3 = 3.75$ mm and center traces of width 10 μ m with 6 μ m gap to ground which gives the characteristic impedances $Z_1 = Z_2 = Z_3 = 50 \Omega$.

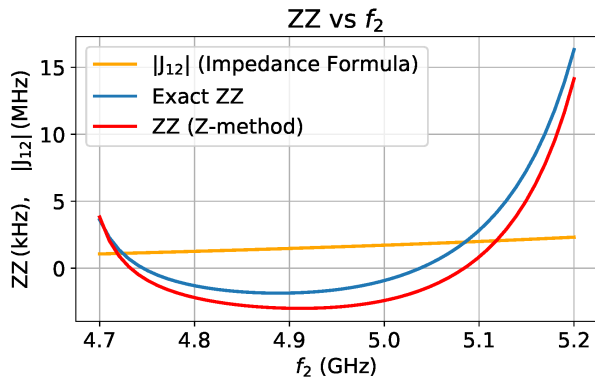


Figure 7. ZZ-interaction rate (blue and red) and the exchange coupling rate J_{12} (orange) for the coupler shown in Fig. (6) as functions of the second qubit's frequency with the first qubit set to 5.0 GHz. We again compare the exact value of the ZZ-rate to the value calculated by the impedance method applying the formula in Eq. (24) using the Eqs. (18)-(23) and adding the cross-Kerr term in Eq. (25) together with the α_{ii} corrections (26)-(27). We observe good agreement at such a low level of ZZ-curves and in the location of the first zero of ZZ-curves that happen at ~ 4.75 GHz. The second ZZ zeros are slightly off as we approach the mode at ~ 6.3 GHz. We included the plot of the exchange coupling J_{12} which is slowly increasing over the qubit band and reaches 2 MHz at ~ 5.10 GHz.

$\lambda/4$ CPW resonator. These two branches run in parallel and are connected to the same Transmon qubit pads as shown in Fig. (6). The $\lambda/4$ section generates a mode at ~ 6.3 GHz. In Fig. (7) we plot ZZ-interaction rate for qubits coupled by the circuit in Fig. (6). ZZ-rate admits two zeros at ~ 4.75 GHz and ~ 5.04 GHz and remains small in magnitude in between which is the typical qubit band.

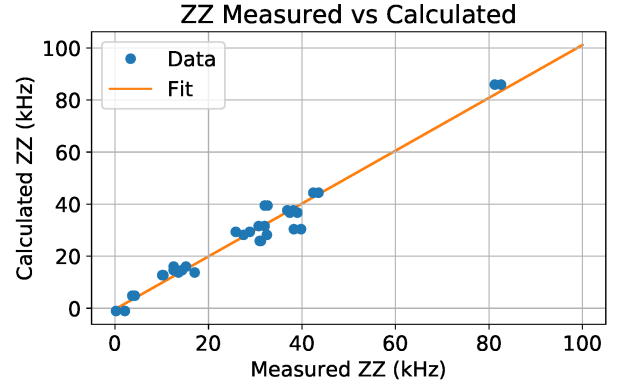


Figure 8. Scatter plot of the measured ZZ values in the multi-qubit chip F609_C where qubit frequencies are spread over the band 4.8 – 5.0 GHz. The least squares fit in orange line has equation $y = 1.015x - 0.388$. The standard deviation is $\sigma = 3.7$ kHz. For each data point x -value corresponds to the measured value whereas the y -value is the ZZ-rate calculated using the impedance method. ZZ-rates measured from both directions are included in the plot for each pair.

V. EXPERIMENTAL RESULTS

In this section we test the validity of the analytical methods we developed in the previous sections on the measurement data collected from real devices. In Figs. (8) and (9) we compare the ZZ values predicted by our method to the measured values from two different multi-qubit devices with qubit frequencies spread over two different frequency bands: on chip F609_C qubit frequencies fall in the band 4.8 – 5.0 GHz whereas qubits on chip F608_C lie between 5.0 – 5.2 GHz. Each chip contains 27 Transmon qubits connected by the ZZ-cancellation type couplers introduced in [20]. We studied this type of coupler in Section (IV C) as an example to compare the results obtained by our analytical method to the exact ZZ-rate values computed by the full-diagonalization of the circuit Hamiltonian. Note that the ZZ-cancellation effect is not observed since the cancellation band is missed in these chips. The coupler topology stays the same across the chip in the sense that all couplers consist of two short $\lambda/2$ CPW arms in parallel with one of the arms shorted to ground in the middle with a $\lambda/4$ CPW section. However the length and the characteristic impedance of the arms and the resonance frequency of the $\lambda/4$ resonator differ creating 6 different coupler responses which allows us to validate of our analytical methods over a larger ensemble with the good agreement seen in Figs. (8) and (9). The calculated ZZ-values are obtained using the Z_{12} output of the 2.5D microwave simulations evaluated at the qubit frequencies. Self-capacitances C_{J_i} 's of the Josephson junctions are extracted (from the anharmonicity data) to be 3.0 fF for the chip F609_C and 2.2 fF for the chip F608_C as the chip F609_C had junctions with larger area.

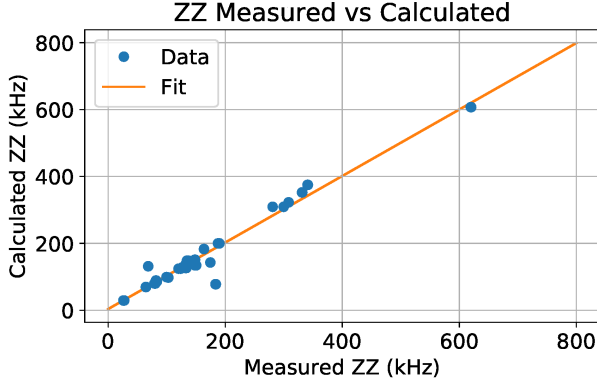


Figure 9. Scatter plot of the ZZ-values for the Chip F608_C. ZZ-values are larger by almost an order of magnitude compared to the chip F609_C in Fig. (8) since qubit frequencies are higher (in the band 5.0 – 5.2 GHz). The least squares fit line is given by $y = 0.994x + 3.71$. The standard deviation is $\sigma = 28.5$ kHz. Again ZZ-rates measured from both directions are included in the plot for each pair when available.

VI. CONCLUSION

We described a method for the accurate calculation of the ZZ-rates between superconducting qubits in the multi-mode circuit-QED. By relating the ZZ-interaction rates directly to the impedance entries connecting the qubit ports our method allows streamlined analysis and design of the qubit-qubit couplers with the help of microwave simulations. In particular this opens a path for the design of higher-order multi-pole ZZ-cancellation couplers by avoiding computationally intensive multi-mode quantum Hamiltonian diagonalization.

Acknowledgements. F. S. acknowledges support from Intelligence Advanced Research Projects Activity (IARPA) under contract W911NF-16-1-0114-FE.

VII. APPENDIX

A. Derivation of the expressions for α_{ij} , α_{ii} and δ_i

The expressions given in Eqs. (17) and (26) for the coefficients α_{ij} and α_{ii} can be derived by expanding the total coordinate transformation $\boldsymbol{\alpha} = \mathbf{T} \exp(\mathbf{S})$ given in [1] to second-order in \mathbf{S} . Here $\boldsymbol{\alpha}$, \mathbf{T} and \mathbf{S} are all $(N + M) \times (N + M)$ matrices where N is the number of qubits and M is the number of the internal modes. The coordinate transformation \mathbf{T} is defined in Eq. (21) of [1] as

$$\mathbf{T} = \begin{pmatrix} \mathbf{1}_{N \times N} & \mathbf{C}_0^{1/2} \mathbf{R}^T \\ \mathbf{0}_{M \times N} & \mathbf{1}_{M \times M} \end{pmatrix} \quad (29)$$

where \mathbf{C}_0 is the diagonal matrix of Transmon capacitances (C_1, \dots, C_N) and $\mathbf{R} = [r_{ik}]$ is the $N \times M$ turns-ratio matrix of the multiport Belevitch transformers in the canonical multiport Cauer network used in [1]. The matrix \mathbf{S} defines the Schrieffer-Wolff transformation $\exp(\mathbf{S})$ that block-diagonalizes the matrix \mathbf{M}_1 defined in Eq. (23) of [1] by

$$\begin{aligned} \mathbf{M}_1 &= \mathbf{T}^T \mathbf{C}_0^{-1/2} \mathbf{M}_0 \mathbf{C}_0^{-1/2} \mathbf{T} \\ &= \begin{pmatrix} \boldsymbol{\Omega}_J^2 & \boldsymbol{\Omega}_J^2 \mathbf{C}_0^{1/2} \mathbf{R}^T \\ \mathbf{R} \mathbf{C}_0^{1/2} \boldsymbol{\Omega}_J^2 & \boldsymbol{\Omega}_{R'}^2 \end{pmatrix} \end{aligned} \quad (30)$$

where $\boldsymbol{\Omega}_J$ is the $N \times N$ diagonal matrix holding the qubit frequencies whereas the $M \times M$ matrix $\boldsymbol{\Omega}_{R'}$ corresponds to the subspace of the internal modes. \mathbf{M}_0 is the diagonal matrix with entries $(1/L_1, \dots, 1/L_N, 1/L_{R_1}, \dots, 1/L_{R_M})$ where L_i 's are qubit inductances for $1 \leq i \leq N$ and $L_{R_k} = 1/\omega_{R_k}^2$ are the inductances of the internal modes for $1 \leq k \leq M$.

After expanding $\exp(\mathbf{S})$ to second-order in \mathbf{S} using for example Eqs. (B.12) and (B.15) in [27] we obtain the expressions in Eqs. (17) and (26) for the coefficients α_{ij} and α_{ii} from the (i, j) and (i, i) entries, respectively, of the upper-left $N \times N$ subsector of $\mathbf{T} \exp(\mathbf{S})$ corresponding to the qubit subspace.

The updated expression in Eq. (27) for the anharmonicity δ_i can be derived by noting that the capacitance re-scaling performed by the diagonal matrix $\mathbf{C}_0^{-1/2}$ can be lumped into the total coordinate transformation $\boldsymbol{\alpha}$ which would re-normalize the diagonal capacitance C_i by $1/\alpha_{ii}^2$ hence the charging energy $E_C^{(i)}$ gets updated by the prefactor α_{ii}^2 ; i.e. $E_C^{(i)} \rightarrow \alpha_{ii}^2 E_C^{(i)}$. One then obtains $\delta_i = -\frac{\alpha_{ii}^2 E_C^{(i)}}{1-2\alpha_{ii}^2 E_C^{(i)}/\omega_i}$ for the anharmonicity using the updated charging energy in the formula given in Eq. (3).

B. Derivation of the expressions for J_{δ_i} and J_{δ_j}

The expression given in Eq. (18) for J_{δ_i} is obtained by noting that the term $\hat{b}_i^\dagger \hat{b}_j^\dagger \hat{b}_i \hat{b}_j$ and its Hermitian conjugate $\hat{b}_i^\dagger \hat{b}_i^\dagger \hat{b}_j \hat{b}_j$ which have weight $\delta_i \sqrt{\frac{\omega_i}{\omega_j}} \alpha_{ij}$ in the expansion \hat{H}_β given in Eq. (16) (\hat{b} denotes qubit operators in Eq. (16)) couple the state $|20\rangle$ to the state $|11\rangle$ with strength $\sqrt{2} \delta_i \sqrt{\frac{\omega_i}{\omega_j}} \alpha_{ij}$. This brings an additive correction to the main coupling $\sqrt{2} J_{ij}$ between the states $|20\rangle$ and $|11\rangle$ generated by the exchange coupling J_{ij} given by the expression in Eq. (5) between qubits i and j ; i.e. $J_{\delta_i} = J_{ij} + \delta_i \sqrt{\frac{\omega_i}{\omega_j}} \alpha_{ij}$. After re-arrangement we arrive at the expression given in Eq. (18) for J_{δ_i} . A similar analysis applied to the terms $\hat{b}_j^\dagger \hat{b}_i^\dagger \hat{b}_j \hat{b}_i$ and $\hat{b}_i^\dagger \hat{b}_j^\dagger \hat{b}_j \hat{b}_i$ (with weight $\delta_j \sqrt{\frac{\omega_j}{\omega_i}} \alpha_{ji}$) for the coupling between the states $|02\rangle$ and $|11\rangle$ gives the expression in Eq. (19) for J_{δ_j} .

[1] Firat Solgun, David P. DiVincenzo and Jay M. Gambetta, "Simple Impedance Response Formulas for the Dispersive Interaction Rates in the Effective Hamiltonians of Low Anharmonicity Superconducting Qubits", *IEEE Transactions on Microwave Theory and Techniques*, Volume: 67, Issue: 3, March 2019.

[2] A. D. Córcoles, E. Magesan, S. J. Srinivasan, A. W. Cross, M. Steffen, J. M. Gambetta and J. M. Chow, "Demonstration of a quantum error detection code using a square lattice of four superconducting qubits," *Nat. Commun.*, vol. 6, p. 6979, (2015).

[3] Sarah Sheldon, Easwar Magesan, Jerry M. Chow, Jay M. Gambetta, "Procedure for systematically tuning up crosstalk in the cross resonance gate", *Phys. Rev. A* 93, 060302 (2016).

[4] Maika Takita, A. D. Córcoles, Easwar Magesan, Baleegh Abdo, Markus Brink, Andrew Cross, Jerry M. Chow, Jay M. Gambetta, "Demonstration of weight-four parity measurements in the surface code architecture", *Phys. Rev. Lett.* 117, 210505 (2016).

[5] Takita, M., Cross, A. W., Córcoles, A. D., Chow, J. M. & Gambetta, J. M. Experimental Demonstration of Fault-Tolerant State Preparation with Superconducting Qubits. *Phys. Rev. Lett.* 119, (2017).

[6] Neereja Sundaresan, Isaac Lauer, Emily Pritchett, Easwar Magesan, Petar Jurcevic, Jay M. Gambetta, "Reducing unitary and spectator errors in cross resonance with optimized rotary echoes", *PRX Quantum* 1, 020318 (2020).

[7] A. Yu. Kitaev, "Fault-tolerant quantum computation by anyons", *Annals Phys.* 303 (2003) 2-30.

[8] Christopher Chamberland, Guanyu Zhu, Theodore J. Yoder, Jared B. Hertzberg, and Andrew W. Cross, "Topological and Subsystem Codes on Low-Degree Graphs with Flag Qubits", *Phys. Rev. X* 10, 011022 (2020).

[9] J. M. Gambetta, J. M. Chow and M. Steffen, "Building logical qubits in a superconducting quantum computing system," *npj Quantum Information*, vol. 3, p. 2, (2017).

[10] G. Catelani, R. J. Schoelkopf, M. H. Devoret, L. I. Glazman, "Relaxation and frequency shifts induced by quasi-particles in superconducting qubits", *Phys. Rev. B* 84, 064517 (2011).

[11] Jens Koch, Terri M. Yu, Jay Gambetta, A. A. Houck, D. I. Schuster, J. Majer, Alexandre Blais, M. H. Devoret, S. M. Girvin, R. J. Schoelkopf, "Charge insensitive qubit design derived from the Cooper pair box", *Phys. Rev. A* 76, 042319 (2007).

[12] Alexandre Blais, Ren-Shou Huang, Andreas Wallraff, S. M. Girvin, R. J. Schoelkopf, "Cavity quantum electrodynamics for superconducting electrical circuits: an architecture for quantum computation", *Physical Review A* 69, 062320 (2004).

[13] Alexandre Blais, Arne L. Grimsmo, S. M. Girvin, Andreas Wallraff, "Circuit Quantum Electrodynamics", *Rev. Mod. Phys.* 93, 25005 (2021).

[14] Jay M. Gambetta, "Control of Superconducting Qubits" in *Quantum Information Processing Lecture Notes*, 44th IFF Spring School 2013, Forschungszentrum Jülich.

[15] Easwar Magesan, Jay M. Gambetta, "Effective Hamiltonian models of the cross-resonance gate", *Phys. Rev. A* 101, 052308 (2020).

[16] Pranav S. Mundada, Gengyan Zhang, Thomas Hazard, Andrew A. Houck, "Suppression of Qubit Crosstalk in a Tunable Coupling Superconducting Circuit", *Phys. Rev. Applied* 12, 054023 (2019).

[17] Fei Yan, Philip Krantz, Youngkyu Sung, Morten Kjaergaard, Dan Campbell, Joel I.J. Wang, Terry P. Orlando, Simon Gustavsson, William D. Oliver, "A tunable coupling scheme for implementing high-fidelity two-qubit gates", *Phys. Rev. Applied* 10, 054062 (2018).

[18] Jaseung Ku, Xuexin Xu, Markus Brink, David C. McKay, Jared B. Hertzberg, Mohammad H. Ansari, B.L.T. Plourde, "Suppression of Unwanted ZZ Interactions in a Hybrid Two-Qubit System", *Phys. Rev. Lett.* 125, 200504 (2020).

[19] A. D. K. Finck, S. Carnevale, D. Klaus, C. Scerbo, J. Blair, T.G. McConkey, C. Kurter, A. Carniol, G. Keefe, M. Kumph, O.E. Dial, "Suppressed crosstalk between two-junction superconducting qubits with mode-selective exchange coupling", *arXiv:2105.11495*.

[20] A. Kandala, K. X. Wei, S. Srinivasan, E. Magesan, S. Carnevale, G. A. Keefe, D. Klaus, O. Dial, D. C. McKay, "Demonstration of a High-Fidelity CNOT for Fixed-Frequency Transmons with Engineered ZZ Suppression", *Phys. Rev. Lett.* 127, 130501 (2021).

[21] Michele C. Collodo, Johannes Herrmann, Nathan Lacroix, Christian Kraglund Andersen, Ants Remm, Stefania Lazar, Jean-Claude Besse, Theo Walter, Andreas Wallraff, Christopher Eichler, "Implementation of Conditional-Phase Gates based on tunable ZZ-Interactions", *Phys. Rev. Lett.* 125, 240502 (2020).

[22] Yuan Xu, Ji Chu, Jiahao Yuan, Jiawei Qiu, Yuxuan Zhou, Libo Zhang, Xinsheng Tan, Yang Yu, Song Liu, Jian Li, Fei Yan, Dapeng Yu, "High-fidelity, high-scalability two-qubit gate scheme for superconducting qubits", *Phys. Rev. Lett.* 125, 240503 (2020).

[23] Ji Chu, Fei Yan, "Coupler-Assisted Controlled-Phase Gate with Enhanced Adiabaticity", *arXiv:2106.00725*.

[24] K. X. Wei, E. Magesan, I. Lauer, S. Srinivasan, D. F. Bogorin, S. Carnevale, G. A. Keefe, Y. Kim, D. Klaus, W. Landers, N. Sundaresan, C. Wang, E. J. Zhang, M. Steffen, O. E. Dial, D. C. McKay, A. Kandala, "Quantum crosstalk cancellation for fast entangling gates and improved multi-qubit performance", *arXiv:2106.00675*.

[25] Firat Solgun, "Microwave Engineer's Guide to the Design of Superconducting Qubit Circuits", *IEEE MTT-S International Microwave Symposium (IMS)*, 263-266, (2019).

[26] S. E. Nigg, H. Paik, B. Vlastakis, G. Kirchmair, S. Shankar, L. Frunzio, M. H. Devoret, R. J. Schoelkopf, and S. M. Girvin, "Black-box superconducting circuit quantization," *Phys. Rev. Lett.*, vol. 108, no. 240502, Jun. 2012.

[27] Roland Winkler, "Quasi-Degenerate Perturbation Theory," in *Spin-Orbit Coupling Effects in Two-Dimensional Electron and Hole Systems*, Berlin, Heidelberg, Germany: Springer-Verlag, 2003, pp. 201-205.